Sensitivity of Flavin Fluorescence Dynamics in Neuronal Nitric Oxide Synthase to Cofactor-Induced Conformational Changes and Dimerization†

Klemens Brunner,‡ Andreas Tortschanoff,‡ Benjamin Hemmens,§ Penelope J. Andrew,§ Bernd Mayer,§ and Andreas J. Kungl*,‖

Institut für Physikalische Chemie, Universität Wien, Währingerstrasse 42, A-1090 Wien, Austria, and Institut für Pharmakologie und Toxikologie and Institut für Pharmazeutische Chemie, Universität Graz, Universitätsplatz 1, A-8010 Graz, Austria

Received May 15, 1998; Revised Manuscript Received September 30, 1998

ABSTRACT: The fluorescence intensity of the two flavin prosthetic groups, FMN and FAD, in neuronal nitric oxide synthase (nNOS) was found to decay highly nonexponentially, being best described by four fluorescence lifetimes. This excited state heterogeneity is the result of multiple flavin quenching sites which are due to several flavin microenvironments created mainly by stacking with aromatic amino acids. Investigating nNOS in the absence of one or more of Ca^{2+}/calmodulin, tetrahydrobiopterin, and heme revealed an influence of these cofactors on the microenvironments of the flavin prosthetic groups. Similar effects on the flavin rotational dynamics were found by analyzing the fluorescence anisotropy decay of the holo and of the different apo forms of nNOS. Since the tetrahydrobiopterin and the heme are located in the N-terminal oxygenase domain of nNOS, their effect on the flavins in the C-terminal reductase domain is explained by a folding back of the reductase domain onto the oxygenase domain. Thereby a domain−domain interface is created containing the FAD, FMN, heme, and tetrahydrobiopterin prosthetic groups which allows for efficient electron transfer during catalysis. The heme group, which is known to be essential for homodimerization of nNOS, was also found to be essential for the formation of the domain−domain interface.

The paramagnetic radical nitric oxide (NO)[1] exerts its diverse physiological effects depending on the local concentration. At high concentrations NO takes part in host defense against tumor cells and pathogens, whereas at low concentrations it acts as a signaling molecule in processes such as vasodilatation and neurotransmission (*1*−*3*). The chemical reactivity of NO in solution is fundamental for its function in vivo (*4*, *5*). It has been shown that NO reacts as a free radical with species containing unpaired electrons such as molecular oxygen, superoxide anion, and metals, leading to formation of a variety of nitrogen oxides (e.g., NO_2, N_2O_3) and peroxynitrite, which act as nitrating and nitrosating agents, respectively. The heme prosthetic group of soluble guanylate cyclase in vascular smooth muscle cells is the major target for the physiological effects of NO released from adjacent endothelial cells, thereby raising the intracellular level of cGMP and leading to vasodilatation (*6*).

NO is enzymatically synthesized from L-arginine by the oxidation of a terminal guanidino nitrogen to give citrulline and NO. Three nitric oxide synthase (NOS) isoforms have been identified based on their mode of activation and their tissue specificity. Constitutively expressed NOS isoforms are activated by an intracellular Ca^{2+} increase, and they therefore produce short pulses of NO. Among the constitutive isoforms are endothelial NOS (eNOS), which mediates blood vessel dilatation (*7*), and neuronal NOS (nNOS), which is involved in cell-to-cell communication in the brain (*8*). On the other hand, inducible NOS (iNOS), to which calmodulin is bound already at very low calcium concentrations, is expressed upon stimulation with cytokines and bacterial products such as lipopolysaccharide (*9*). Although the NOS isoforms differ in their molecular size, 160 kDa for nNOS and 130 kDa for iNOS, they were all found to be homodimers sharing a modular monomer architecture with identical cofactors and prosthetic groups (*10*, *11*). The N-terminal cytochrome P450-like oxygenase domain, which contains heme, tetrahydrobiopterin (H_4B), and the L-arginine binding site, is linked via a calmodulin binding domain to the C-terminal cytochrome P450 reductase-like domain, which contains FAD, FMN, and the NADPH binding site. The binding sites of the NOS cofactors and prosthetic groups have been identified by site-directed mutagenesis experiments and by sequence alignment studies with homologous proteins (*12*).

The three-dimensional structure of the NOS reductase domain can be approached by a close inspection of the recently solved X-ray structure of the highly homologous

† This work was supported by the Oesterreichische Nationalbank (Grant 246 to A.J.K. and Grant 6655 to B.M.) and by the Fonds zur Förderung der Wissenschafflichan Forschung (Grant P12566-PHY to K.B. and A.T. and Grant P11478 to B.M.).

* To whom correspondence should be addressed at the Institut für Pharmazeutische Chemie, Universität Graz, Universitätsplatz 1, A-8010 Graz, Austria. Telephone: +43-316-380/5373. Fax: +43-316-382541. E-mail: andreas.kungl@kfunigraz.ac.at.

‡ Institut für Physikalische Chemie, Universität Wien.

§ Institut für Pharmakologie und Toxikologie, Universität Graz.

‖ Institut für Pharmazeutische Chemie, Universität Graz.

[1] Abbreviations: NO, nitric oxide; nNOS, neuronal nitric oxide synthase; CPR, cytochrome P450 reductase; H_4B, tetrahydrobiopterin; PBS, phosphate-buffered saline.

10.1021/bi981138l CCC: $15.00
Published on Web 11/20/1998

NADPH−cytochrome P450 reductase (CPR) (*13*). The authors reported a modular molecular architecture of trypsinolysed CPR consisting of four structural domains: a single domain for each cofactor/prosthetic group, NADPH, FAD and FMN, and a FAD−FMN connecting domain. Both flavins were found to be stacked with aromatic amino acid side chains, thereby keeping the flavins tightly bound to the protein. Recently, the X-ray structure of a dimeric iNOS oxygenase truncation mutant containing H_4B, L-arginine, or the product analogue thiocitrulline was reported by Crane et al. (*14*). Compared to the earlier reported H_4B-free, monomeric iNOS oxygenase structure (*15*), the presence of the pterin was found to massively refold the central interface region, thereby creating a 30 Å deep channel and exposing a heme edge. This cavity was suggested to be the likely contact surface for the interaction with the NOS reductase domain. The substrate L-arginine was found to bind to Glu-371 and to be stacked with heme in a hydrophobic pocket.

Since only limited structural information on intact, dimeric NOS is available, we have undertaken time-resolved fluorescence studies on fully active and structurally intact dimeric nNOS in solution. Over the past few years, time-resolved fluorescence spectroscopy has turned out to be a very sensitive and efficient method to explore structural details of proteins (*16*). The spectral as well as the temporal characteristics of protein-intrinsic fluorophores, such as aromatic amino acids and flavins, are dependent on their local environment (*17*, *18*). Therefore, recording the steady-state and the time-resolved fluorescence spectra yields valuable insights into microstructural details of the protein. This is of special interest for investigating the structural changes of a protein upon ligand binding (*19*) or upon folding/refolding (*20*). In addition, recording the time-resolved fluorescence anisotropy of a chromophore-containing protein enables the investigation of the microstructural dynamics of the fluorophore and its surrounding as well as the measurement of the overall rotation of the entire macromolecule (*21*). Commonly, fluorescence experiments are carried out at low micromolar or even nanomolar concentrations, and experiments usually take from a few minutes up to a few hours. This means that, compared to X-ray crystallography and NMR spectroscopy, fluorescence spectroscopy reveals microstructural details of a chromophore's environment at very low chromophore concentrations and within rather short times.

In the present study, we have investigated the time-resolved fluorescence properties of the flavin prosthetic groups of nNOS, with special emphasis on the microstructural and dynamic differences of calmodulin-, H_4B-, and heme-containing nNOS relative to the calmodulin-, H_4B -, and heme-free forms of the protein. The results are interpreted as intramolecular communication between the reductase and oxygenase domains which is sensed by the flavin fluorescence dynamics.

MATERIALS AND METHODS

nNOS Purification. Production and purification of recombinant rat brain NOS from a baculovirus overexpression system was accomplished according to published protocols (*22*). The expression and purification of H_4B- and heme-deficient forms of nNOS was also described recently (*23*, *24*). Calmodulin and H_4B were purchased from Sigma (Steinheim, Germany) and were used without further purification. Before and after the fluorescence experiments the activity of the enzyme was determined by measuring nitrite production with the Griess assay (*25*) or with a modified fluorescence method using 2,3-diaminonaphthalene (*26*). For all fluorescence measurements, the enzyme was diluted from a concentrated stock solution into phosphate-buffered saline (PBS) containing 137 mM NaCl, 2.7 mM KCl, 4.3 mM Na_2HPO_4, 1.4 mM KH_2PO_4, pH 7, giving a final concentration of 2 μM nNOS. All fluorescence measurements were performed at 21 °C.

Steady-State Fluorescence Spectra. The steady-state fluorescence spectra were recorded on a LS50B fluorometer from Perkin Elmer (Beaconsfield, England). Slit widths of 2 nm were used, and the spectra were corrected for background emission.

Absorbance Spectra. Absorption spectra of nNOS were recorded on a Hewlett-Packard 8452A diode-array spectrophotometer (Hewlett-Packard, Palo Alto, CA) using quartz cuvettes with a path length of 1 cm.

Time-Resolved Fluorescence Spectroscopy. The fluorescence transients of nNOS were recorded according to the single-photon counting (SPC) technique (*27*). The details of the SPC setup have been described elsewhere (*26*, *28*). In short, the sample was excited at 400 nm with the second harmonic of a 120 fs laser pulse (fwhm 10 nm) which was generated by an Ar^+-pumped, Kerr-lens modelocked Mira 900F Ti:Sapphire laser (Coherent, Santa Clara, CA). The high repetition rate of the laser (76 MHz) was reduced to 4.75 MHz by inserting a pulse-picker (Model 9200, Coherent) in the beam path. To exclude scattered light due to the excitation pulse as well as due to Raman scatter from the sample emission, cutoff filters (GG 495, OG515 from Schott, Mainz, Germany) were inserted in the fluorescence path before spectral selection by a single-grating monochromator (Model 1681, Spex, Edison, NJ). The signal was detected by a Peltier-cooled MCP 3809U multichannel plate from Hamamatsu (Shimokanzo, Japan). The output of the MCP was further processed by a GHz preamplifier (Model 9306, Ortec, Oak Ridge, TN) and a fast constant fraction discriminator (Model 9307, Ortec). The negative logic pulse from this discriminator was used to start a voltage ramp in the time-to-amplitude converter, which was stopped in the reversed SPC mode by the next incoming signal from the laser-triggered photodiode. For fluorescence intensity decay measurements (i) the emission was collected with magic angle position of the emission polarizer or (ii) the total decay was computed from the *G*-factor corrected sum of the horizontally and perpendicularly polarized emission components (see below). Commonly, $(4 \times 10^5)-(1 \times 10^6)$ counts in the peak channel maximum were collected.

For the time-resolved anisotropy measurements, a liquid crystal variable retarder (Meadowlark Optics, Colorado) was placed in the excitation beam path to control the excitation laser beam polarization. Since polarized laser experiments are sensitive to cumulative artifacts such as laser-output instabilities, wavelength drifts, and sample degradation, the vertically and horizontally polarized fluorescence components were acquired alternately by a computer-controlled polarizer allowing typically 20 s per position of the polarizer. A total of 30−60 cycles were generally needed to obtain a satisfac-

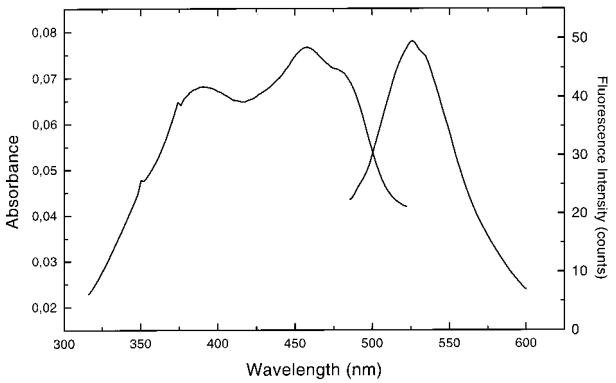

FIGURE 1: Absorption and fluorescence emission spectra of nNOS. The displayed absorption spectrum was recorded with a 2 μM heme-free nNOS solution in 10 mM triethanolamine/HCl, pH 7.4, 0.1 M NaCl. The fluorescence emission spectrum was recorded with a 2 μM holo-nNOS solution in PBS (see Materials and Methods) at 21 °C with the excitation wavelength set at 387 nm.

tory time-resolved anisotropy data quality. The initial anisotropy of the protein was found to be lower than expected (see Figure 5) due to excitation of the sample at 400 nm in the region between the two absorption bands of nNOS (see Figure 1).

The time-resolved fluorescence intensity as well as the anisotropy raw data were analyzed by iterative reconvolution using the FLA900 program from Edinburgh Instruments (Edinburgh, U.K.). The leading edge of the fluorescence intensity decay was always included in the analysis to account for very short lifetime components. Commonly, a multiexponential model for the intensity and anisotropy transients was applied, assuming independently emitting, noninterconverting species. This kind of discrete exponential analysis yielded in principle the same values (lifetimes and rotational correlation times) as in a distributional analysis (data not shown). The quality of the fits was judged by examing the reduced value of χ^2, the randomness of the weighted residuals, and the autocorrelation function. By this method of data recording and processing, an overall time resolution of approximately 10 ps was achieved.

RESULTS

In Figure 1, the absorption and the steady-state fluorescence emission spectra of the flavin prosthetic groups, FAD and FMN, of nNOS are shown. For a better inspection of the flavin absorption bands and to exclude the dominant heme absorption band, the absorption spectrum of heme-deficient nNOS (*24*) is presented. The absorption as well as the emission transitions found for nNOS closely resemble the flavin spectra of other flavin-containing proteins (*29*, *30*). Two absorption bands at 390 nm and at 457 nm correspond to a dominant fluorescence emission band at 525 nm. The pronounced shoulder in the absorption spectrum at 480 nm is interpreted in analogy to the work of van den Berg et al. (*30*) as being due to a charge-transfer interaction of the flavin(s) with a neighboring tyrosine residue (see below). Of the two flavin prosthetic groups found in nNOS, the major part of the emission is expected to result from FMN because of its inherently higher fluorescence quantum yield, *Q*, in solution compared to FAD: *Q*(FMN) = 0.26 and *Q*(FAD) = 0.03 (*31*, *32*). Although the fluorescence emission of both FAD and FMN is due to the isoalloxazine ring, the emission of FAD is frequently intramolecularly quenched by stacking with the adenine moiety (*33*). Commonly, the fluorescence emission of flavins bound to proteins is strongly quenched, rendering the detection of the fluorescence signal difficult. In nNOS the total flavin fluorescence intensity was found to be quenched by a factor of 8 compared to a FAD:FMN = 1:1 mixture.

To determine the extent of free flavins in the nNOS preparations used for the fluorescence measurements, ultrafiltered nNOS solutions were chromatographed using reversed phase HPLC and flavin standard solutions as reference (see Figure 2) (*34*). By this means, the free FMN content was found to be 0.2% ± 0.003% (relative to the protein concentration), and the content of free FAD was below the detection limit of our system (≤0.02%). Despite the very low content of free flavins, their contribution to the time-resolved fluorescence of nNOS has to be kept in mind when interpreting the enzyme's transient fluorescence patterns (see below).

The time-resolved flavin fluorescence intensity decay of a 2 μM nNOS solution in PBS is shown in Figure 3. This enzyme preparation contained the cofactor Ca^{2+}/calmodulin, and the prosthetic groups FAD, FMN, heme, and H_4B and will therefore be referred to as holo-nNOS. The excitation wavelength for the time-resolved fluorescence experiments was chosen to be 400 nm because of maximum laser excitation power, and the fluorescence transients were collected at 525 nm. To check whether the enzyme was photophysically or photochemically degraded during the laser experiments, the activity of the enzyme solution before and after the laser experiments was confirmed to be the same by the detection of nitrite production with the Griess assay (*25*) or with a time-resolved fluorescence assay (*26*) (data not shown).

The highly nonexponential fluorescence decay of holo-nNOS (Figure 3) was best fitted by four fluorescence lifetimes which are summarized in Table 1. To illustrate the quality of the fit, the weighted residuals and the autocorrelation function, which both exhibit a random distribution around zero, were incorporated in Figure 3. By visually inspecting the nNOS flavin fluorescence transients, the rapidly decaying initial phase is immediately obvious (see Figures 3 and 4). A predominant ultrafast fluorescence lifetime, τ_1 = 31 ps (see Table 1), was identified for this flavin quenching path, the absolute amplitude of which is ca. 30 times higher than each of the remaining decay constants. In analogy to the ultrashort lifetime component found for the quenched FAD fluorescence in gluthathione reductase (*30*), τ_1 of the nNOS decay is interpreted as being the result of photoinduced electron transfer from a neighboring tyrosine residue to an excited isoalloxazine ring. This is in agreement with the pronounced shoulder at 480 nm found in the nNOS flavin absorption spectrum which is the result of an isoalloxazine ring coupling electronically with a tyrosine residue in the ground state (see Figure 1). τ_2 and τ_3 both have much smaller amplitudes compared to τ_1 (see Table 1) and are thus most probably due to less populated, differently quenched states of FAD and/or FMN. Different microenvironments which do not interconvert on a fluorescence time scale were assumed to be responsible for the multiple quenching sites of the flavin prosthetic groups.

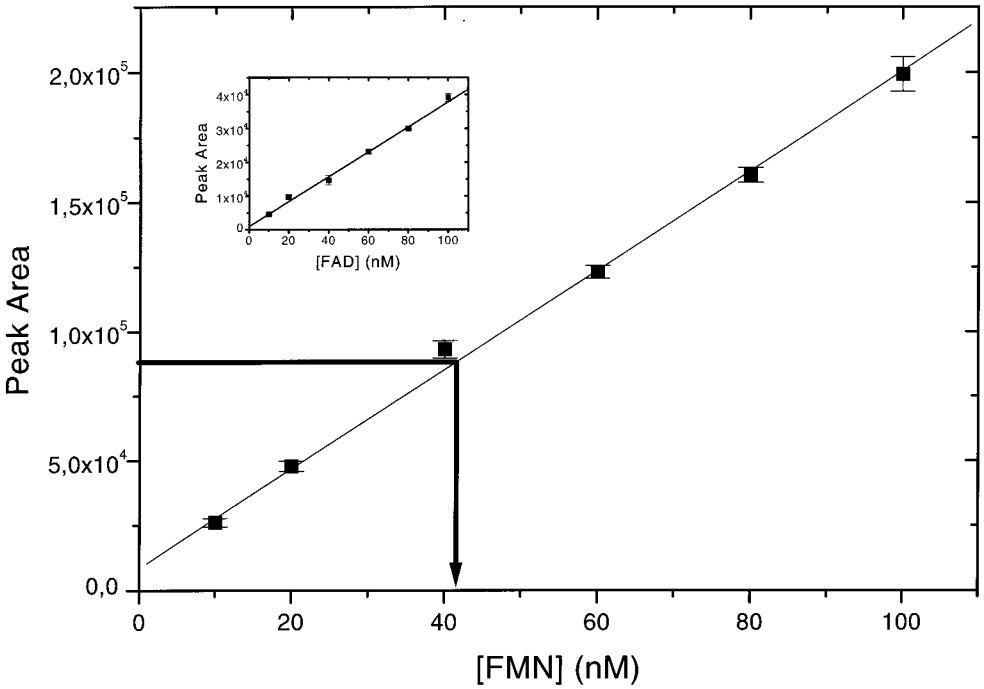

FIGURE 2: Determination of free FMN and FAD (insert) of a 21.3 μM nNOS solution. After ultrafiltration of a fresh nNOS preparation, the flavin content of the eluate was determined by reversed-phase HPLC using flavin standards as reference (details of the method are described in ref *34*). The data shown represent the mean values from three independent determinations. The free FMN concentration was found to be 40.6 $\pm$ 0.5 nM (indicated by the bold arrow), corresponding to 0.2% $\pm$ 0.003% of the enzyme concentration, whereas the free FAD concentration was below the detection limit ($\leq$5 nM).

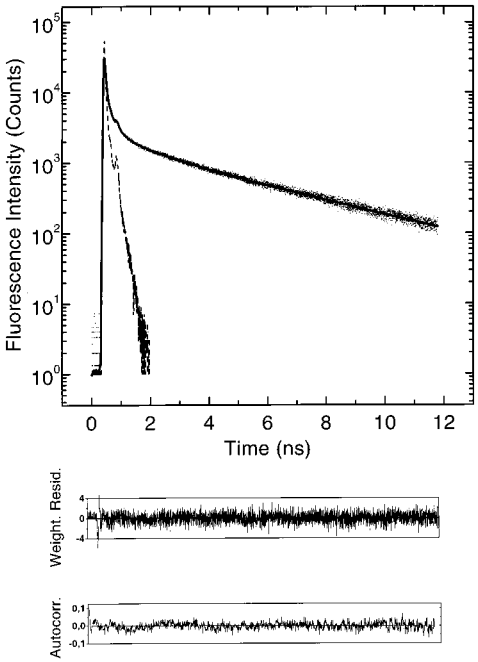

FIGURE 3: Time-resolved fluorescence intensity decay of a 2 μM holo-nNOS solution at 21 °C in PBS (see Materials and Methods). The excitation wavelength was set at 400 nm, and the emission was collected at 525 nm. The fluorescence raw data are represented as dots, the best (multiexponential) fit is displayed as a solid line, and the instrument response function is shown as a dashed line.

The long fluorescence lifetime of holo-nNOS, $\tau_4 = 5.07$ ns (see Table 1), is comparable in range to the intrinsic lifetime of FMN ($\tau_{FMN} = 4.33$ ns, see Table 1). It therefore seemed reasonable to interpret τ_4 as the intrinsic lifetime of FMN which is increased relative to its value in solution as a result of a local hydrophobic microenvironment within nNOS. This environment shields the excited FMN chromophore from solvent and side chain collisions and thus extends its lifetime. The intrinsic fluorescence lifetime of the very low fraction of unbound FMN (see Figure 2) could not be resolved as an individual component of the nNOS fluorescence intensity decay. However, applying distributional analysis (contained within the FLA900 program from Edinburgh Instruments; see Materials and Methods) to the fluorescence intensity decay of nNOS revealed a broad fluorescence lifetime distribution centered around τ_4 (the remaining three lifetimes were obtained as discrete values with no significant distributional width; data not shown). It is therefore suggested that the minor contribution of the free flavins is contained within the fluorescence lifetime distribution centered around τ_4. This distribution, which is commonly interpreted as being the result of conformational substates interacting differently with the excited chromophore(s), becomes broader due to the contribution of the free flavins. However, it is mainly the changes in the nNOS fluorescence decay parameters upon the presence or absence of cofactors and substrate which will be discussed in the following. The influence of the very low fraction of free flavins on the biological conclusions is thus expected to be negligible.

Binding of L-arginine to holo-nNOS had no significant influence on the flavin fluorescence intensity decay (see Table 1). Analysis of the fluorescence decay obtained from nNOS without the cofactor Ca^{2+}/calmodulin revealed a decreased value of $\tau_4 = 4.31$ ns. In addition, the relative amplitude, A_1, of the ultrafast component increased significantly (see Table 1). Both effects are illustrated in Figure 4 in which the raw fluorescence data have been omitted for clarity, and the multiexponential fit of the nNOS holoenzyme decay is compared with the fits of the different apo forms. A decreased value of τ_4 means, according to our interpreta-

Table 1: Parameters of the Multiexponential Reconvolution of the nNOS Flavin Fluorescence Intensity Decay[a]

	A_1 (%)	τ_1 (ps)	A_2 (%)	τ_2 (ps)	A_3 (%)	τ_3 (ns)	A_4 (%)	τ_4 (ns)	$\langle\tau\rangle$ (ns)	χ^2
nNOS(−Ca^{2+}/calm)	20.96	27 ± 0.3	7.75	149 ± 5	11.88	0.94 ± 0.02	59.42	4.31 ± 0.02	2.69 ± 0.01	1.188
holo-nNOS	12.66	31 ± 0.3	6.78	232 ± 6	17.45	1.38 ± 0.03	63.1	5.07 ± 0.04	3.46 ± 0.02	1.162
holo-nNOS(+L-Arg)	11.88	33 ± 0.3	6.41	250 ± 6	16.49	1.42 ± 0.04	65.22	5.03 ± 0.03	3.53 ± 0.02	1.086
nNOS(−H_4B)	15.95	27 ± 0.2	4.14	163 ± 5	6.81	1.08 ± 0.04	73.1	4.25 ± 0.01	3.19 ± 0.01	1.099
nNOS(−H_4B)(+Ca^{2+}/calm)	12.1	32 ± 0.2	2.96	207 ± 9	6.74	1.22 ± 0.05	78.2	4.35 ± 0.01	3.49 ± 0.01	1.144
nNOS(−heme)	2.46	40 ± 0.4	1.9	447 ± 12	95.64	3.31 ± 0.01			3.18 ± 0.01	1.147
nNOS(−heme)(+Ca^{2+}/calm)	1.77	33 ± 0.8	2.25	566 ± 24	95.97	3.32 ± 0.01			3.20 ± 0.01	1.165
FAD	1.33	27 ± 0.7	30.59	1745 ± 24	68.08	3.24 ± 0.02				1.240
FMN	100	4332 ± 2								1.114

[a] The relative amplitudes A_i were calculated according to A_i (%) = $[(A_i\tau_i)/(\sum A_i\tau_i)] \times 100$.

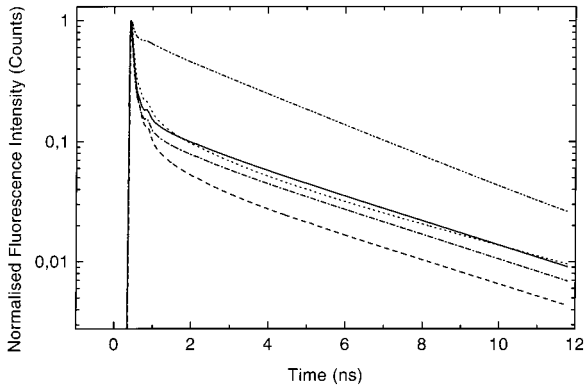

FIGURE 4: Comparison of the multiexponential fluorescence intensity decay fits of different nNOS forms: (− •• −) heme-free nNOS; (•••) holo-nNOS; (—) H_4B-free Ca^{2+}/calmodulin-containing nNOS; (− • −) H_4B-free nNOS; (− −) Ca^{2+}/calmodulin-free nNOS.

tion, that the microenvironment which shielded the FMN from solvent and/or side chain collisions in the holoenzyme becomes more solvent-exposed in the Ca^{2+}/calmodulin-free form of nNOS. In addition, the fraction of nNOS molecules with a strongly quenched flavin fluorescence decay, represented by A_1, increased relative to the holo-enzyme. Binding of Ca^{2+}/calmodulin to nNOS clearly induced significant structural changes in the flavin binding sites, thereby changing the quenching site pattern.

Investigating the Ca^{2+}/calmodulin- and H_4B-free form of nNOS yielded an even lower τ_4 = 4.25 ns. This was accompanied by an over 10% increase of the relative amplitude A_4 and by a 5% decrease of A_1 relative to the Ca^{2+}/calmodulin-free nNOS (see Table 1 and Figure 4). The presence of H_4B, although situated in the oxygenase domain of nNOS, seems to be a prerequisite for certain microstructures of the flavin binding sites in the reductase domain. Adding Ca^{2+}/calmodulin to the Ca^{2+}/calmodulin- and H_4B-free nNOS gave a similar relative amplitude of the ultrafast component, A_1, compared to the holo-enzyme. However, the value of τ_4 did not increase to the holo-enzyme's value, but instead the relative amplitude A_4 increased to 78.2% (see Table 1 and Figure 4). Shaping of the FMN microenvironment, i.e., shielding from collisions with solvent and side chains, obviously needs the presence of both Ca^{2+}/calmodulin and H_4B cofactors.

The steady-state fluorescence intensity of heme-free nNOS was found to be significantly higher relative to the emission of holo-nNOS (data not shown), referring to a contribution of the heme group to the static quenching of the flavins in holo-nNOS. The time-resolved fluorescence intensity decay of heme-free nNOS appeared to be nearly monoexponential with a predominant lifetime of τ_3 = 3.31 ns and two minor lifetime components with relative amplitudes below 3% (see Figure 4 and Table 1). Heme-deficient nNOS was shown to be monomeric, to lack H_4B, and to have a normal flavin content and cytochrome *c* reductase activity (*24*). The dominant fluorescence lifetime can therefore be due either to similarly quenched FMN and FAD chromophores or to a solely emitting flavin, the other one being completely statically quenched and thus not contributing at all to the fluorescence decay. In heme-free nNOS, the characteristic ultrafast component is almost completely missing in the fluorescence decay, with only a residual amount of 2.5% detectable (see Table 1 and Figure 4). Binding of Ca^{2+}/calmodulin to heme-free nNOS had no detectable effect on the fluorescence decay of the flavins. The flavin microenvironments situated in the reductase domain of nNOS are thus sensitive to Ca^{2+}/calmodulin binding only in the presence of heme.

A direct measure of a chromophore's dynamics is the time-resolved fluorescence anisotropy (*21*). By this means, the rotational correlation motions of the fluorophore(s) which depolarize(s) the plane-polarized exciting light are revealed. Commonly the fluorescence anisotropy decay of protein-intrinsic chromophores is described by two rotational correlation times, referring to the local chromophore motion on the one hand and to the overall rotation of the protein on the other hand, both of which are occurring on different time scales. As an alternative to depolarization by rotational dynamics, the fluorescence can be depolarized by resonance energy transfer to an energetically suitable acceptor chromophore or by the formation of a charge-transfer complex. Both mechanisms are dependent upon the relative position of the energy/charge donating and accepting group.

The flavin fluorescence anisotropy of nNOS was found to decay very rapidly to zero (see Figure 5), being best described by two rotational correlation times, ϕ_1 = 316 ps and ϕ_2 = 2.35 ns (see Table 2). On the basis of an empirical formula (*35*), a rotational correlation time of 120 ns at 20 °C would have been expected for the overall rotation of nNOS. No such correlation time was detected (see Table 2 and Figure 5), independent of the time window chosen for the anisotropy experiments (data not shown). This was apparently due to the fast initial decay of the fluorescence intensity, rendering the signal insufficient to detect long rotational correlation times. Both decay times were found to decrease with increasing temperature (see Table 2). Although the time scale of ϕ_1 corresponds to fast relaxation dynamics of the flavin prosthetic groups within their micro-

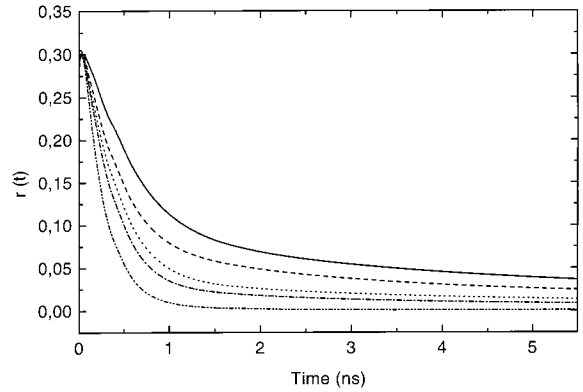

FIGURE 5: Comparison of the multiexponential anisotropy decay fits of different nNOS forms: (—) Ca^{2+}/calmodulin-free nNOS; (− −) holo-nNOS; (•••) H_4B-free nNOS; (− • −) H_4B-free Ca^{2+}/calmodulin-containing nNOS; (− •• −) heme-free nNOS.

environments, depolarization due to the formation of a charge-transfer complex between (an) excited flavin(s) and (a) neighboring aromatic amino acid(s) (*30*) seems to be the more likely reason for the fast fluorescence depolarization (ϕ_1) of nNOS. Both processes, conformational dynamics and charge-transfer formation, are expected to occur with a higher rate at higher temperatures. However, the dominant ultrashort fluorescence lifetime (τ_1), which was attributed to charge-transfer quenching by neighboring aromatic amino acids (see above), is an indication that this process is also responsible for the fast depolarization mode of nNOS. The long rotational correlation time of nNOS, ϕ_2, is interpreted as being the result of a slow rotational depolarization within the nNOS molecule, such as the movement of a protein segment, rather than energy transfer between FAD and FMN, since the latter process is expected to be independent of temperature.

The anisotropy decay of holo-nNOS was affected only marginally by binding of the substrate L-arginine (see Table 2), which is similar to its marginal effect on the nNOS fluorescence intensity decay (see Table 1). In Ca^{2+}/calmodulin-free nNOS, both relaxation times were found to be significantly slower compared to the holo-enzyme (see Table 2 and Figure 5). These data suggest that binding of Ca^{2+}/calmodulin had a direct or an indirect influence on the flavin binding sites thereby modulating both depolarizing modes of the nNOS flavin emission. In H_4B-free nNOS which did not contain Ca^{2+}/calmodulin, ϕ_1 was found to be 300 ps and ϕ_2 was found to equal 2.76 ns. In addition, the relative contributions (amplitudes) of these two depolarizing modes to the overall anisotropy decay were reversed compared to the holoenzyme (see Table 2). Adding Ca^{2+}/calmodulin to the H_4B-free nNOS resulted in a decrease of ϕ_2 to 2.11 ns, referring to a similar segmental mobility compared to the holoenzyme. However, the amplitude ratio of the rotational correlation times remained opposite to the ratio found for the holoenzyme (see Table 2), indicating that this ratio and therefore the population of specific depolarization states is determined by the presence of H_4B.

The anisotropy recorded for the heme-free, monomeric form of nNOS was found to decay much faster compared to the holoenzyme. Two subnanosecond rotational correlation times were again detected, but both were much shorter than in all other nNOS forms (see Table 2). The flavin dynamics seemed thus much less restricted in heme-free nNOS which was accompanied by, or which was the result of, the flavins losing contact to their charge-transfer partners. Although the heme-free form of nNOS binds Ca^{2+}/calmodulin, as shown by the detection of cytochrome P450 reductase activity (*24*), the addition of Ca^{2+}/calmodulin to the heme-free nNOS had no effect on the flavin fluorescence anisotropy decay (see Table 2 and Figure 5).

DISCUSSION

Unravelling the structural details of an enzyme greatly enhances the understanding of its mechanism. Since recombinant NOS isoforms became available in large quantities, several groups have tried to crystallize and to solve the structure of this important enzyme. Recently, the X-ray structure of the dimeric iNOS oxygenase domain containing heme, H_4B, and arginine was reported (*14*). However, no structural information is available on the interaction between the NOS oxygenase and the reductase domain. In the underlying study, we have therefore undertaken time-resolved fluorescence studies on the nNOS reductase-bound flavins, FAD and FMN, which were found to be influenced by the absence or presence of prosthetic groups contained within the nNOS oxygenase domain. We obtained evidence for a structural domain−domain communication within nNOS which is essential for electron transfer and thus for biological activity of the enzyme.

Multiexponential fluorescence decays have frequently been observed for flavoproteins (*29*, *30*, *36*, *37*). These complex decay patterns are generally difficult to interpret in molecular photophysical terms. The nNOS enzyme preparations used for this study were carefully characterized before and after the measurements, and the content of free flavins was found to be very low (see Figure 2). Overall structural homogeneity was thus assumed. However, microstructural heterogeneity of the flavin sites may account for the nonexponential fluorescence decay of nNOS. The four fluorescence lifetimes of the nNOS flavin fluorescence decay were therefore interpreted as being due to multiple quenching sites of FAD and FMN. This means that specifically populated microconformations for these chromophores exist which do not interconvert on a fluorescence time scale and therefore contribute to the fluorescence decay as individually fluorescing molecules.

From the recently solved crystal structure of NADPH−cytochrome P450 reductase (CPR) (*13*), which is highly homologous to the C-terminal, flavin-containing, reductase domain of nNOS, it can be seen that both flavin chromophores, FAD and FMN, are stacked between aromatic amino acids. In CPR, FMN is covered by Tyr140 on the *re*-face and by Tyr178 on the *si*-face, whereas FAD is covered by Tyr456 on the *si*-face and by Trp677 on the *re*-face. These amino acids are highly conserved among the CPR family, including nNOS. According to the sequence homology between CPR and nNOS, we therefore expect stacking of the nNOS FMN prosthetic group with the aromatic residues Phe810 and Tyr890, whereas the FAD group should be stacked with Tyr1176 and by Phe1396. Stacking with aromatic amino acids is one obvious reason for different flavin fluorescence quenching channels within nNOS. In a recent publication, van den Berg et al. (*30*) suggested electron transfer to be a common mechanism for

Table 2: Parameters of the Multiexponential Reconvolution of the nNOS Flavin Fluorescence Anisotropy Decay[a]

	T (°C)	B_1 (%)	ϕ_1 (ps)	B_2 (%)	ϕ_2 (ns)	r_∞	$\langle\phi\rangle$ (ns)	χ^2
nNOS(−Ca^{2+}/calm)	10	33.87	555 ± 22	66.13	3.55 ± 0.62	0.02	2.53 ± 0.41	1.005
	21	33	418 ± 19	67	3.22 ± 0.56	0.021	2.23 ± 0.38	0.965
	25	38.06	360 ± 11	61.94	2.81 ± 0.40	0.01	1.87 ± 0.25	0.979
	30	43.61	276 ± 7	56.39	2.17 ± 0.24	0.004	1.34 ± 0.13	0.951
holo-nNOS	21	39.83	316 ± 10	60.17	2.35 ± 0.26	0.017	1.53 ± 0.15	1.055
holo-nNOS(+L-Arg)	21	40.29	300 ± 8	59.71	2.34 ± 0.23	0.016	1.51 ± 0.13	1.028
nNOS(−H_4B)	21	57.81	300 ± 6	42.19	2.76 ± 0.52	0.008	1.34 ± 0.22	1.001
nNOS(−H_4B)(+Ca^{2+}/calm)	21	65.16	250 ± 4	34.84	2.12 ± 0.37	0.006	0.90 ± 0.13	1.011
nNOS(−heme)	21	86.78	180 ± 2	13.22	0.75 ± 0.13	0.0007	0.255 ± 0.017	1.096
nNOS(−heme)(+Ca^{2+}/calm)	21	81.98	164 ± 2	18.02	0.750[b]	0.003	0.269 ± 0.002	1.059
FAD	21	100	185 ± 2			0.002		1.085
FMN	21	100	154 ± 2			0		0.954

[a] The relative amplitudes B_i were calculated according to B_i (%) = $[(B_i\phi_i)/(\sum B_i\phi_i)] \times 100$. [b] This rotational correlation time had to be kept fixed during the analysis to obtain an adequate fit.

flavin quenching by juxtapositioned tyrosine residues. This photoinduced electron transfer is the most probable reason for the ultrafast component, τ_1, detected in the nNOS flavin fluoresecence decay, as well as for the fast depolarization term, ϕ_1, found in the anisotropy decay. Since both flavin prosthetic groups are likely to be stacked with a tyrosine residue, it is not possible to unambiguously associate the electron-transfer process to a certain flavin. It cannot be ruled out that both flavin groups have the potential to accept electrons from the neighboring tyrosine residue in the excited state. On the other hand, the hydrophobic non-charge-transfer interaction between FMN and Phe810 might be the reason for the increased intrinsic fluorescence lifetime, τ_4, of FMN in holo-nNOS compared to the isolated fluorophore.

Besides the interactions of FAD and FMN with the highly conserved aromatic amino acids phenylalanine and tyrosine, which themselves offer the possibility of multiple quenching channels, the cysteine residue at position 894 in nNOS might be responsible for an additional quenching site. Cys894 is the nNOS homologue replacement of the asparagine residue at position 182 of CPR, which is in close vicinity to the FMN isoalloxazine ring. Cysteine residues are known to be able to efficiently quench the flavin fluorescence (*38*). Together with the aromatic amino acids expected to stack with the flavins (see above), a multitude of quenching channels for the flavin prosthetic groups in nNOS are assumed, which appear to be the reason for the nonexponential nNOS fluorescence decay.

Regardless of the exact nature of these quenching mechanisms, we have detected an influence of the cofactors H_4B, heme, and Ca^{2+}/calmodulin on the flavin microconformations as well as on the microstructural dynamics. The biological activity of nNOS is strictly dependent on the binding of Ca^{2+}/calmodulin which triggers interdomain electron transfer between the flavins and heme (*39*). Binding of Ca^{2+}/calmodulin to nNOS is inhibited by a synthetic peptide corresponding to the amino acid sequence 830−870 from nNOS (*40*). This sequence is located in the FMN binding domain of nNOS and is absent in the inducible isoform of NOS to which calmodulin is bound already at very low Ca^{2+} concentrations (*41*). In analogy to other calmodulin binding proteins, it was therefore proposed, that upon activation by increased Ca^{2+} concentrations, calmodulin must displace an inhibitory loop from the vicinity of its nNOS binding site, which is supposed to be the amino acid region 830−870 (*40*). From a comparison with the known FMN binding domain of CPR, the conserved amino acids Phe810 and Tyr890 are expected to stack with the FMN prosthetic group in nNOS (see above). Since these two amino acids are right at the core of the proposed inhibitory loop, it seemed reasonable to assume that displacing the inhibitory loop by binding of Ca^{2+}/calmodulin creates a different microenvironment for FMN. This was further manifested in the anisotropy decays of Ca^{2+}/calmodulin-containing and Ca^{2+}/calmodulin-free nNOS. The rotational correlation time ϕ_2 was suggested to correspond to a flavin-containing segmental motion. From the crystal structure of CPR, it can be seen that the FMN domain is connected to the rest of the enzyme via a so-called hinge region, which was not well ordered in the crystal structure, suggesting a higher mobility of the FMN domain. Since a similar overall fold of the nNOS reductase domain compared with CPR can be expected, the ϕ_2 rotational correlation time of the nNOS aniostropy decay most likely results from a hinge-bend movement of the FMN domain. As FMN is assumed to be rigidly bound to the protein (by stacking with aromatic amino acids), rotational relaxation occurs mainly through the hinge-bend motion of the FMN domain. Binding of Ca^{2+}/calmodulin to nNOS decreased the value of ϕ_2, indicating an altered hinge-bend motion of the FMN domain. In addition, the fluorescence lifetime τ_4, which was interpreted as the intrinsic lifetime of FMN being shielded from solvent and matrix collisions within the holoenzyme, was found to be similar to the value of the FMN lifetime in solution when the Ca^{2+}/calmodulin-free nNOS was investigated (see Table 1). This is interpreted as a greater solvent exposure of FMN in the Ca^{2+}/calmodulin-free nNOS similar to the FMN in CPR. In agreement with the effects of Ca^{2+}/calmodulin binding on the nNOS flavin time-resolved fluorescence, Gachhui et al. (*42*) have recently reported an increase of the steady-state flavin fluorescence emission upon Ca^{2+}/calmodulin binding to the recombinantly expressed reductase domain of nNOS.

Interestingly, the H_4B-free nNOS also exhibited different modes and/or contributions of flavin quenching channels compared to the holoenzyme and thus different microenvironments for these chromophores. This refers to a close vicinity of H_4B to the active site of the reductase domain in holo-nNOS. We therefore suggest that in holo-nNOS the reductase domain folds back onto the oxygenase domain, thereby creating a functional domain−domain interface. In the heme-free nNOS, a dramatically different flavin fluorescence and anisotropy decay compared to the holoenzyme

was observed, referring not only to a different population of flavin quenching sites but also to a completely different quenching pattern in heme-free nNOS. The significant but moderate effects observed in the flavin microenvironments of Ca^{2+}/calmodulin- and H_4B-free nNOS compared to the holoenzyme are interpreted as being the result of basically similar, but differently populated, flavin quenching sites which are not present in the absence of heme. We therefore suggest that in the heme-free nNOS monomer the oxygenase domain is no longer folded back onto the reductase domain. The X-ray structure of the iNOS oxygenase domain revealed an exposed heme edge, which the authors suggest to take part in binding of the reductase domain (*14*). Based on our results, we propose that the heme is essential for folding back of the reductase domain onto the oxygenase domain. This domain−domain interface is apparently responsible for specific microenvironments of the nNOS flavin prosthetic groups which become completely insensitive to Ca^{2+}/calmodulin binding in the heme-free nNOS. Since in the X-ray structure of the iNOS oxygenase domain H_4B was found to be localized very close to the heme, the effect of this prosthetic group on the flavin microenvironments suggests that the four prosthetic groups, FAD, FMN, heme, and H_4B, are located in close proximity at the domain−domain interface of intact nNOS. Such a configuration would allow very efficient, direct electron transfer from the flavins to the heme. The participation of H_4B in the electron-transfer process itself still remains unclear. In the active site of the iNOS oxygenase domain the arginine substrate was found to be located "behind" the heme with respect to the domain−domain interface (*14*). Arginine is apparently not involved in the domain−domain interaction. This is reflected by the marginal effect of the arginine substrate on the nNOS flavin microenvironments.

In conclusion, we have utilized time-resolved fluorescence measurements to show that both heme and H_4B, despite binding to the structurally distinct oxygenase domain of nNOS, have a major effect on the fluorescence dynamics of the reductase-bound flavins. This is interpreted as evidence for an interaction between the two separate domains of nNOS to form an oxygenase/reductase domain interface. This heme-dependent conformation is likely to be of major functional importance with respect to electron transfer during catalysis. Hence, this study provides further insight into the unique biochemistry of NOS, with evidence supporting the structural role of the heme, as well as suggesting the close proximity of the four prosthetic groups at the oxygenase/reductase domain interface in the native structure of active, dimeric nNOS.

ACKNOWLEDGMENT

We thank Eva Pitters for helping to prepare the nNOS enzyme and Antonius Gorren for helpful discussions.

REFERENCES

1. Farrell, A. J., and Blake, D. R. (1996) *Ann. Rheum. Dis. 55*, 7−20.
2. Mayer, B., and Hemmens, B. (1997) *Trends Biochem. Sci. 22*, 477−481.
3. Nathan, C. (1995) *Cell 82*, 873−876.
4. Wink, D. A., Grisham, M. B., Mitchell, J. B., and Ford, P. C. (1996) *Methods Enzymol. 268*, 12−31.
5. Stamler, J. S., and Feelisch, M. (1996) in *Methods in Nitric Oxide Research* (Feelisch, M., and Stamler, J. S., Eds.) John Wiley & Sons, New York.
6. Ignarro, L. J. (1989) *Circ. Res. 65*, 1−21.
7. Palmer, R. M., Ashton, D. S., and Moncada, S. (1988) *Nature 327*, 524−526.
8. Bredt, S. D., and Snyder, S. H. (1989) *Proc. Natl. Acad. Sci. U.S.A. 86*, 9030−9033.
9. Xie, Q., Cho, H. J., Calaycay, J., Mumford, R. A., Swiderek, K. M., Lee, T. D., Ding, A., Troso, T., and Nathan, C. (1992) *Science 256*, 225−228.
10. Masters, B. S. S., McMillan, K., Sheta, E. A., Nishimura, J. S., Roman, L. J., and Martasek, P. (1996) *FASEB J. 10*, 552−558.
11. Baek, K. J., Thiel, B. A., Lucas, S., and Stuehr, D. J. (1993) *J. Biol. Chem. 268*, 21120−21129.
12. Liu, Q., and Gross, S. S. (1996) *Methods Enzymol. 268*, 311−324.
13. Wang, M., Roberts, D. L., Paschke, R., Shea, T. M., Masters, B. S. S., and Kim, J.-J. (1997) *Proc. Natl. Acad. Sci. U.S.A. 94*, 8411−8416.
14. Crane, B. R., Arvai, A. S., Ghosh, D. K., Wu, C., Getzoff, E. D., Stuehr, D. J., and Tainer, J. A. (1998) *Science 279*, 2121−2126.
15. Crane, B. R., Arvai, A. S., Gachhui, R., Wu, C., Ghosh, D. K., Getzoff, E. D., Stuehr, D. J., and Tainer, J. A. (1997) *Science 278*, 425−431.
16. Eftink, M. (1991) *Methods Biochem. Anal. 35*, 127−205.
17. Lakowicz, J. R. (1983) *Principles of Fluorescence Spectroscopy*, Plenum Press, New York.
18. Beechem, J. M., and Brand, L. (1985) *Annu. Rev. Biochem. 54*, 43−71.
19. Kungl, A. J., Visser, N. V., van Hoek, A., Visser, A. J. W. G., Billich, A., Schilk, A., Gstach, H., and Auer, M. (1998) *Biochemistry 37*, 2778−2786.
20. Eftink, M. R. (1994) *Biophys. J. 66*, 482−501.
21. Steiner, R. F. (1991) in *Topics in Fluorescence Spectroscopy 2* (Lakowicz, J. R., Ed.) Plenum Press, New York/London.
22. Mayer, B., Klatt, P., List, B. M., Harteneck, C., and Schmidt, K. (1996) *Methods Enzymol. 268*, 420−427.
23. Gorren, A. C. F., List, B. M., Schrammel, A., Pitters, E., Hemmens, B., Werner, E. R., Schmidt, K., and Mayer, B. (1996) *Biochemistry 35*, 16735−16745.
24. Klatt, P., Pfeiffer, S., List, B. M., Lehner, D., Glatter, O., Bächinger, H. P., Werner, E. R., Schmidt, K., and Mayer, B. (1996) *J. Biol. Chem. 271*, 7336−7342.
25. Green, L. C., Wagner, D. A., Glogowski, J., Skipper, P. L., Wishnok, S. R., and Tannenbaum, S. R. (1982) *Anal. Biochem. 126*, 131−138.
26. Andrew, P. J., Auer, M., Lindley, I. J. D., Kauffmann, H. F., and Kungl, A. J. (1997) *FEBS Lett. 408*, 319−323.
27. O'Connor, D. V., and Phillips, D. (1984) *Time-Correlated Single Photon Counting*, Academic Press, London.
28. Kersting, R., Mollay, B., Rusch, M., Wenisch, J., Leising, G., and Kauffmann, H. F. (1997) *J. Chem. Phys. 106*, 2850−2864.
29. Bastiens, P. I. H., Bonants, P. J. M., Müller, F., and Visser, A. J. W. G. (1989) *Biochemistry 28*, 8416−8425.
30. van den Berg, P. A. W., van Hoek, A., Walentas, C. D., Perham, R. N., and Visser, A. J. W. G. (1998) *Biophys. J. 74*, 2046−2058.
31. Weber, G., and Teale, F. W. J. (1957) *Trans. Faraday Soc. 53*, 646−655.
32. Spencer, R. D., and Weber, G. (1972) in *Structure and Function of Oxidation−Reduction Enzymes* (Akeson, A., and Ehrenberg, A., Eds.) Pergamon Press, Oxford.
33. Visser, A. J. W. G. (1984) *Photochem. Photobiol. 6*, 703−706.
34. Klatt, P., Schmidt, K., Werner, E. W., and Mayer, B. (1996) *Methods Enzymol. 268*, 358−365.

35. Visser, A. J. W. G., Penners, N. H. G., and Müller, F. (1983) in *Mobility and Recognition in Cell Biology* (Sund, H., and Veeger, C., Eds.) Walter De Gruyter, Berlin.
36. Visser, A. J. W. G. (1989) in *Fluorescent Biomolecules* (Jameson, D. M., and Reinhardt, G. D., Eds.) Plenum Press, New York.
37. Tanaka, F., Tamai, N., Nakashima, N., and Yoshihara, K. (1989) *Biophys. J. 56*, 901−909.
38. Deonarain, M. P., Scrutton, N. S., Berry, A., and Perham, R. N. (1990) *Proc. R. Soc. London B 241*, 179−186.
39. Abu-Soud, H. M., and Stuehr, D. J. (1993) *Proc. Natl. Acad. Sci. U.S.A. 90*, 10769−10772.
40. Salerno, J. C., Harris, D. E., Irizarry, K., Patel, B., Morales, A. J., Smith, S. M. E., Martasek, P., Roman, L. J., Masters, B. S. S., Jones, C. L., Weissman, B. A., Lane, P., Liu, Q., and Gross, S. S. (1997) *J. Biol. Chem. 272*, 29769−29777.
41. Cho, H. J., Xie, Q.-W., Calaycay, J., Mumford, R. A., Swiderek, K. M., Lee, T. D., and Nathan, C. (1992) *J. Exp. Med 176*, 599−604.
42. Gachhui, R., Presta, A., Bentley, D. F., Abu-Soud, H. M., McArthur, R., Brudvig, G., Ghosh, D. K., and Stuehr, D. J. (1996) *J. Biol. Chem. 271*, 20594−20602.

BI981138L